PCCP

Physical Chemistry Chemical Physics

An international journal

www.rsc.org/pccp

Volume 9 | Number 46 | 14 December 2007 | Pages 6053–6160

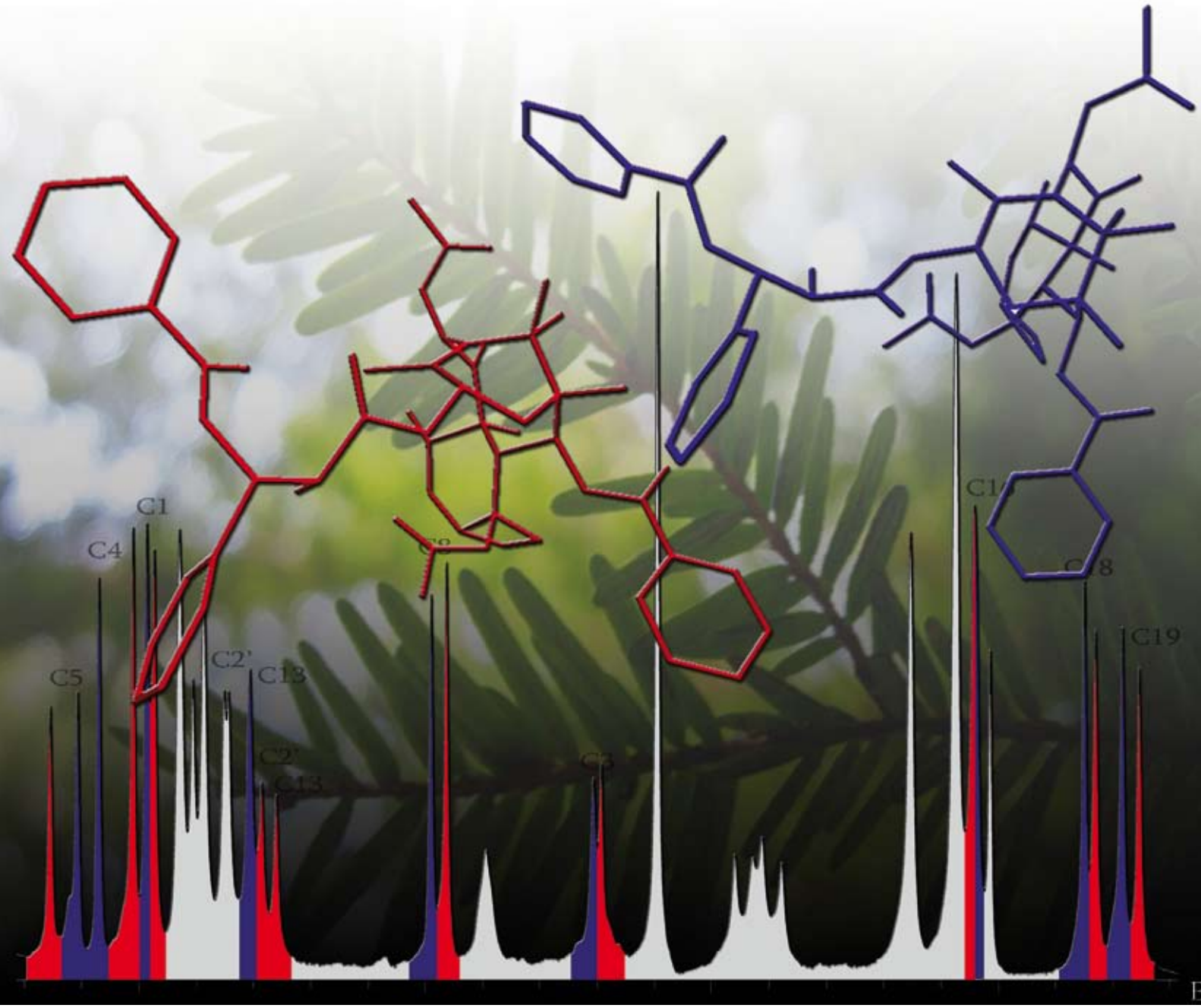

ISSN 1463-9076

1463-9076(2007)9:46;1-9

Structural characterization of an anhydrous polymorph of paclitaxel by solid-state NMR†‡

Elizabeth M. Heider,[ab] James K. Harper[b] and David M. Grant*[b]

Received 19th July 2007, Accepted 18th September 2007
First published as an Advance Article on the web 10th October 2007
DOI: 10.1039/b711027h

The three-dimensional structure of a unique polymorph of the anticancer drug paclitaxel (Taxol®) is established using solid state NMR (SSNMR) tensor (^{13}C & ^{15}N) and heteronuclear correlation (^{1}H–^{13}C) data. The polymorph has two molecules per asymmetric unit ($Z' = 2$) and is thus the first conformational characterization with $Z' > 1$ established solely by SSNMR. Experimental data are correlated with structure through a series of computational models that extensively sample all conformations. For each computational model, corresponding tensor values are computed to supply comparisons with experimental information which, in turn, establishes paclitaxel's structure. Heteronuclear correlation data at thirteen key positions provide shift assignments to the asymmetric unit for each comparison. The two distinct molecules of the asymmetric unit possess nearly identical baccatin III moieties with matching conformations of the C10 acetyl moiety and, specifically, the torsion angle formed by C30–O–C10–C9. Additionally, both are found to exhibit an extended conformation of the phenylisoserine sidechain at C13 with notable differences in the dihedral angles centered around the rotation axes of O–C13, C2′–C1′ and C3′–C2′.

Introduction

Since its discovery in 1971, paclitaxel (Fig. 1) has become a powerful and widely used anticancer agent. Its unique bioactivity promotes the assembly and stabilization of microtubules. Since these stabilized microtubules cannot retract after chromosomal separation, cellular mitosis is terminated. Paclitaxel successfully treats a number of cancers,[1] including breast, ovarian and lung carcinomas.[2] Additionally, paclitaxel has demonstrated efficacy in treating cancers resistant to other therapies,[3] has been used to inhibit smooth muscle cell proliferation and migration for treatment of restinosis,[4] and further applications of paclitaxel are presently under investigation. Enormous clinical success has made paclitaxel the focus of many studies.[5] Despite this attention, relatively little is known about the structure of tubulin-bound paclitaxel and debate continues over which conformation constitutes the bioactive form. Several models dominate the discussion, three of which are considered herein: the nonpolar[6–8] and polar[9–12] forms, and the T-taxol[13,14] conformation.

The nonpolar conformation, observed in nonpolar solvents such as methylene chloride, is proposed to be the likely bioactive conformation on the assumption that the paclitaxel binding site on microtubules is hydrophobic.[6] In this structure, the C2 benzoyl group is found to be closer to the phenyl amide group (~5 Å) than to the C3′ phenyl group (~10 Å).[7] In addition, the H2′–C2′–C3′–H3′ torsion angle is ~60.0°.[8]

The polar form is observed in polar solvents such as water.[9] Both NMR and molecular modeling studies of this form demonstrate that the C3′ phenyl group is positioned close to the C2 benzoyl and C4 acetyl groups (~6 Å)[9] and takes on an H2′–C2′–C3′–H3′ torsion angle of ~180.0°.[8] Ojima *et al.*[10] proposed a particularly detailed polar model, the hydrophobically-collapsed (HC) form. HC is said to occur when "two hydrophobic centers are sufficiently close to exclude an intervening solvent molecule".[11] This conformation with a different binding mode was also found by Li *et al.*[12] by fluorescence

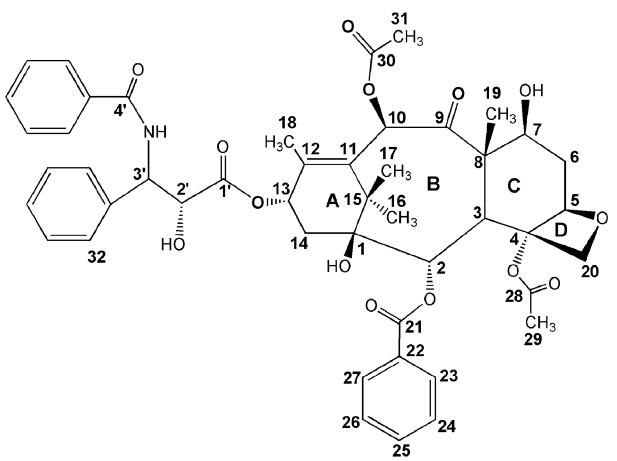

Fig. 1 Structure and numbering of paclitaxel.

[a] *Department of Physics and Astronomy, Tufts University, Medford, MA 02155, USA. Fax: +1 (1)6176273878; Tel: +1 (1)6176273878*
[b] *University of Utah Department of Chemistry, 315 S. 1400 E., Salt Lake City, UT 84112, USA. E-mail: grant@chem.utah.edu; Fax: +1 (1)8015818843; Tel: +1 (1)8015818854*

† Electronic supplementary information (ESI) available: Coordinates of computational models and calculated chemical shielding eigenvalues for retained structures. See DOI: 10.1039/b711027h

‡ **Dedication:** This article is dedicated to the memory of the late Dr David Weaver at Tufts University, a good scientist and generous mentor.

spectroscopy and REDOR NMR studies of a fluorinated paclitaxel derivative.

A third conformer, T-taxol, has recently emerged as a form consistent with the electron crystallographic density studies of paclitaxel bound to the α,β-tubulin dimer,[13] and increased bioactivity was observed in paclitaxel analogs synthetically constrained to mimic this conformation.[14] The T-taxol conformation shares characteristics of the nonpolar form and is extended along the C13 sidechain. Additionally the C2 benzoate group is equidistant from the phenyl rings in the C13 sidechain, resulting in a T-shaped conformation, and the closest H–H separation between the C4 acetate methyl hydrogen and the *ortho*-proton of the C3′ phenyl ring is small (2.5–2.9 Å).

While these proposed conformations provide insight into paclitaxel's structure–activity relationships (SAR), structural analysis *via* single crystal X-ray diffraction is unavailable because paclitaxel does not form suitable crystals from solvents that mimic biological conditions. In fact, there is only one known crystal structure of paclitaxel (Fig. 2) containing two molecules per asymmetric unit (*i.e.* $Z' = 2$ referred to herein as molecules **1a** and **1b**) and crystallizing in the $P2_1$ space group.[15] Moreover, this polymorph is unstable and contains the solvent dioxane, rendering it less useful for biological studies.

This work investigates a second highly-stable microcrystalline paclitaxel polymorph[16] (with $Z' = 2$ referred to herein as **2a** and **2b**) that crystallizes in the $P2_12_12_1$ space group but does not produce crystals suitable for X-ray diffraction analysis. The relatively-large size of this form, combined with two molecules per asymmetric crystallographic unit, and the lack of a single crystal make it unlikely that the structure of this molecule can be determined through conventional diffraction approaches. This study therefore utilizes solid state NMR (SSNMR) spectroscopy to study paclitaxel's structure. This approach is an extension of recently developed SSNMR methods which investigate compounds unsuitable for study by traditional procedures.[23]

SSNMR has been used as a tool to investigate chemical structure and is a sensitive indicator of hydrogen bonding,[17] stereochemistry,[18] conformation,[19] steric forces[20] and electrostatic interactions.[21] Isotropic chemical shift values from liquid NMR and rapid magic angle spinning SSNMR give insight into certain molecular features (*e.g.* stereochemistry) but, because of averaging effects, are often unable to provide more subtle structural details. Comparatively, the chemical shift tensor (CST) with three or six measurable shift values per nucleus[22] yields a three-dimensional map of regional electromagnetic influences. As such, it strongly reflects local geometries and lattice effects, thereby serving as a sensitive probe of structure and conformation. Complete molecular geometries have now been predicted by combining the three chemical shift principal values (CSPV) from the diagonalized shift tensor with *ab initio* calculations.[23] This approach was originally utilized by Oldfield *et al.*[24] and has since been extended and proven to allow successful structural analyses in a variety of molecules.[18,19,23] Likewise, structural predictions have been made utilizing dipolar coupling information combined with computation,[25] and also through the use of spin diffusion models.[26] These studies set a precedent for the use of SSNMR spectroscopy in analyzing solids that would be inaccessible using traditional diffraction procedures.

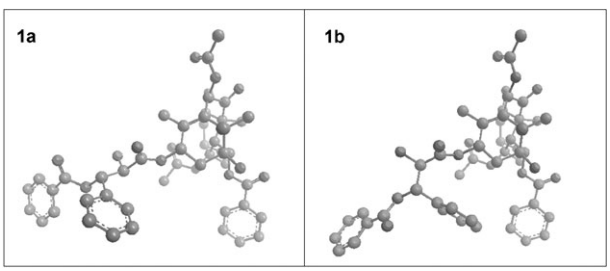

Fig. 2 Conformers **1a** and **1b** present in the asymmetric unit of the X-ray crystal structure of paclitaxel.[15] The sidechain conformation in both molecules is found in the orientation usually associated with polar solvents.

In this paper SSNMR CSPV data are combined with computer modeling to establish the three-dimensional structure of paclitaxel **2**. This computational/experimental approach employs construction of models to sample probable molecular conformations. Through an extension to previous methods,[18] CSPV values are computed for each conformer model, compared with experimental CSPVs, and the model retained or eliminated at a statistical probability. This analysis is possible due to the sensitivity of CSPVs to local features and because the rigidity of paclitaxel's baccatin moiety lessens the burden of a global search of conformation. Furthermore, the ^1H–^{13}C heteronuclear correlation technique (HETCOR) establishes shift assignments,[27] enabling statistical comparison of CSPVs at multiple nuclear locations. It is therefore feasible to ascertain the most probable conformations through SSNMR data.

The proposed structural elucidation of paclitaxel **2** *via* SSNMR is reliant on computer-generated structures. Prior work has demonstrated that, while geometry can be computed with relatively simple models,[28] higher level calculations are needed for computing NMR CST values.[29] Thus, with its substantial diversity of conformational models and relatively larger size, paclitaxel presents considerable obstacles for modeling. The effort of conducting a global search of paclitaxel's conformation is, therefore, aided by developing methods which may address these challenges.

Paclitaxel is well-known for possessing conformational flexibility and paclitaxel analogs have displayed vastly differing geometries. In particular, the C13 phenylisoserine sidechain, long identified as crucial to paclitaxel's bioactivity,[30] can adopt several conformations depending on the substituents at C2′ and C3′ and the nature of the surrounding solvent.[31] Energy methods alone have been found to be insufficient for providing a consistent ranking of known sidechain conformers.[32] In spite of this conformational variation, the baccatin III tetracyclic ring system that forms the major portion of paclitaxel has been shown to be rigid.[33] Prior work[34] has, therefore, suggested that studies of larger systems containing baccatin III moieties could assume a ''typical structure'' without introducing significant errors. Analyses of the CSPVs of **A**–**D** rings of taxanes confirm this finding.[34] Because the baccatin moiety provides a rigid segment of

paclitaxel, the conformational freedom in this molecule is considerably reduced, with the sidechains at C10 and C13 representing the only significant segments of unknown geometry in paclixtaxel. Modeling that emphasizes these sidechains greatly decreases the number of computations otherwise required.

Complications caused by the molecular size of paclitaxel were further alleviated by a systematic approach that exploits the short-range nature of the NMR chemical shift tensor. Because tensor values primarily reflect local structure,[35] some parts of the molecule may therefore be conformationally-frozen or even eliminated without influencing the tensors in distant fragments. Typically, atoms more than three bonds distant or a few Å from a given position have little influence on tensors. This allows construction of a set of structurally-truncated models that represent isolated segments of paclitaxel, yet yield accurate CSPVs with a shorter computation time (Fig. 3). This method was employed to perform a global conformation search for **2** as well as to calculate the values for single-crystal data for which no published CSPVs exist.

While these treatments alleviate computational difficulties, an additional challenge is presented in analysis of **2** due to the two molecules in the asymmetric unit. When $Z' = 2$, pairs of resonances are observed at different frequencies for a single molecular position because the two molecules are geometrically inequivalent and experience different local environments. Accordingly, pairs of CSPVs are obtained for most positions. While prior methods[18,34] can correctly assign shifts to appropriate molecular position, additional data are needed to assign a given tensor to a specific **a** or **b** molecule. Recently, progress has been made in this area with the use of a proton–carbon heteronuclear correlation (HETCOR) experiment using Lee–Goldburg homonuclear decoupling.[27] In this work, shifts for 2 molecules with $Z' = 2$ were assigned to the asymmetric unit using HETCOR. In all cases the HETCOR assignments were found to match established assignments known from independent SSNMR data. Thus, HETCOR was used herein to assign more than 70% of the CSPVs in the C13 sidechain to a particular molecule in the asymmetric unit.

Accurate assignment of shifts to the asymmetric unit provides a distinct benefit in ascertaining conformation. Since CSPVs from a single carbon may fit several models equally well, it is advantageous to combine data from additional nuclear positions. By combining CSPVs from neighboring atoms within three bonds (*i.e.* the γ position) of a given carbon, one may effectively eliminate the ambiguity from a CSPV comparison at a single position.[36] When the CSPVs are unassigned to a specific **a** and **b** molecule, however, combining information from multiple positions is not an option and this advantage no longer exists.

Experimental

All 1D ^{13}C isotropic spectra of paclitaxel were acquired on a Chemagnetics CMX400 spectrometer using the TOSS pulse sequence[37] and a 7.5 mm probe. Analyses were performed with TPPM decoupling[38] using a 180° pulse of 8.3 μs and a phase angle variation of ±8° between adjacent pulse segments. The spectra were acquired with a spectral width of 40.0 kHz, an operating frequency of 100.621 MHz and a decoupling frequency of 400.121 MHz. Other acquisition parameters included ^{1}H and ^{13}C 90° pulses of 4.3 and 4.4 μs, respectively, a pulse delay of 4.0 s, a spinning speed of 4.0 kHz, a cross-polarization time of 3.0 ms, and a digital resolution of 9.7 Hz per point. The spectra were referenced to the high-frequency peak of adamantane at 38.56 ppm.

FIREMAT data were obtained using a spinning speed of 950 Hz, a TPPM phase angle of ±18°, and a cross polarization time of 1.5 ms. A total of 32 evolution increments of 1920 scans each were collected with evolution and acquisition spectral widths of 17.54 and 105.26 kHz, respectively. A digital resolution of 8.2 Hz per point was obtained in the acquisition dimension. The digital resolution of the evolution dimension of 4.7 Hz per point was realized after data replication and rearrangement employed in the FIREMAT analysis.[39] Tensor principal values were extracted using previously described software and techniques.[39] All other parameters were identical to those listed for the TOSS analysis.

The HETCOR analysis was performed on a wide-bore 600 MHz Varian Infinity spectrometer using a 4.0 mm probe and the pulse sequence of van Rossum *et al.*[40] Spectra were acquired at ^{13}C and ^{1}H frequencies of 150.834 and 599.796 MHz, respectively. Other acquisition parameters included ^{13}C and ^{1}H spectral widths of 35.997 and 15.107 kHz, a spinning speed of 13.0 kHz, a B_1 decoupling field strength of 119.0 KHz, a pulse delay of 4.0 s and TPPM decoupling[38] in the acquisition dimension. Lee–Goldburg ^{1}H–^{1}H decoupling[41] was used during the evolution period and consisted of a 1.9 μs 90° ^{1}H pulse and

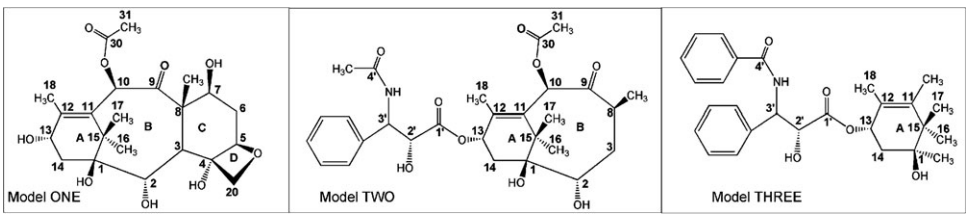

Fig. 3 Models of truncated paclitaxel used in the calculations of conformers of **2**. Note that, since little variation exists between the X-ray determined dihedral angles of the baccatin core in multiple analogs, the need to define conformation of the complete ring system is eliminated. Thus, models contain selected regions for **A**, **B**, **C**, and **D** rings obtained from 10-deacetyl baccatin III and no model includes the complete baccatin moiety.

four Lee–Goldburg cycles per evolution increment. A total of 128 evolution points of 128 scans each were collected for an experimental time of 18.3 h. The digital resolution in the evolution and acquisition dimensions were 118.0 and 32.7 Hz per point, respectively. A dataset with a short cross polarization time of 70 μs was acquired to identify protons covalently attached to carbons. Three additional datasets were subsequently acquired with longer cross-polarization times of 130, 180 and 240 μs, to identify ^{13}C sites at increasingly greater distances from a given ^{1}H. The ^{1}H dimension was referenced to a non-spinning sample of liquid DMSO in a sealed capillary at 2.49 ppm. The ^{13}C dimension was referenced to the high frequency peak of adamantane at 38.56 ppm. All reported proton shifts were scaled by 0.577 as required for Lee–Goldburg homonuclear decoupling.[40]

A total of 650 conformationally-varied model structures were constructed on a computer to systematically sample all feasible sidechain and C10-acetyl conformations. Similar modeling of the baccatin III moiety was avoided by assuming a typical structure of the **A**–**D** rings based on prior work.[34] All sidechain structures were geometry optimized with certain conformational constraints (see discussion below in Computational modeling) using the AM1 method[42] and NMR shift tensors were subsequently computed at the B3PW91/D95** level of theory[43] using Gaussian 03.[44] Prior work on the closely related molecule 10-deacetyl-baccatin III found errors in the computed principal values to be 4.22 ppm.[34] Conversion of shielding to shift was determined by making plots of sp^2 and sp^3 carbon shielding *versus* shift for the principle values of 10-deacetyl-baccatin III previously published.[34] The plots were linear and gave conversions of shift = (shielding − 186.86)/(−1.0215) with $r^2 = 0.986$ for sp^2 carbons and $r^2 = 0.984$ and shift = (shielding − 185.88)/(−1.0285) for sp^3 carbons. The fact that a least-squares fit gives a slope different than unity indicates a systematic error in the computed tensors. These errors are accounted for by using the slope values listed and provide the best-fit for the data. The systematic errors in the computations are different (larger) in sp^2 carbons than the sp^3 sites due to the challenge of treating electron correlation effects. The use of separate slope and intercept values for sp^2 and sp^3 carbons is intended to correct for this difference. Insufficient ^{15}N tensor values were available to determine slope and intercept conversion values as done for ^{13}C. Thus a slope of unity was assumed and the computed chemical shielding values of the nitrogen in the C13 sidechain were converted to shift according to the ^{15}N shift of liquid CH_3NO_2 given by Jameson, *et al.*[45] as shift = −(shielding + 135.8). All shift values were converted using the icosahedral method of Alderman *et al.*[46] which provide the proper weight to each shift component for CSPV measurement under magic angle turning. In the assessment of calculated structure to experimental data, an icosahedral distance was used as the rms error according to a previously described procedure.[21]

Structures of highest probability were selected by comparing computed tensor principal values to experimental data using a statistical method described earlier.[18,23] Enhancements to this method are described herein.

Results and discussion

^{13}C Shift assignments when $Z' > 1$

Structural analysis *via* NMR requires correct assignment of chemical shifts to a specific molecular location. This is particularly difficult in paclitaxel, however, since two molecules per asymmetric unit are present.[16] Thus, in addition to assignment of a shift to a molecular position, an assignment to the correct asymmetric unit is needed.

Typical assignment methods, such as comparison to solution shifts or computed shifts,[47] are therefore not germane since each position gives two resonances with nearly identical shift values. In a limited number of cases, the solid-state INADEQUATE, UC2QF-COSY or spin diffusion methods[48] have been used to obtain assignments to the asymmetric unit.

However, these techniques are usually applicable only to solids with isotopic labelling, short relaxation times or moderate molecular weights. In practice, these methods have only been applied to compounds with molecular weights less than 390 g mol^{-1} and are therefore less suited for analysis of paclitaxel with a formula weight of 853.9 ($\sim$1708 for $Z' = 2$). An alternative is the ^{1}H–X HETCOR experiment[49] which has recently been demonstrated to provide sufficient resolution to assign shifts to a specific molecule of the asymmetric unit.[27]

Shift assignments in paclitaxel were made through a series of ^{1}H–^{13}C correlation spectra and were acquired with gradually increasing cross-polarization (CP) times and a pulse sequence that transfers magnetization *via* dipolar couplings.[49d] Protons bonded to carbons were identified by collecting a 70 μs CP spectrum that only allowed magnetization transfer over very short distances and was therefore dominated by bonded ^{1}H–^{13}C pairs. In subsequent spectra, with CP times of 130, 180 & 240 μs, a total of 28 through-space correlations not observed at 70 μs were found, corresponding to the positions illustrated in Fig. 4.

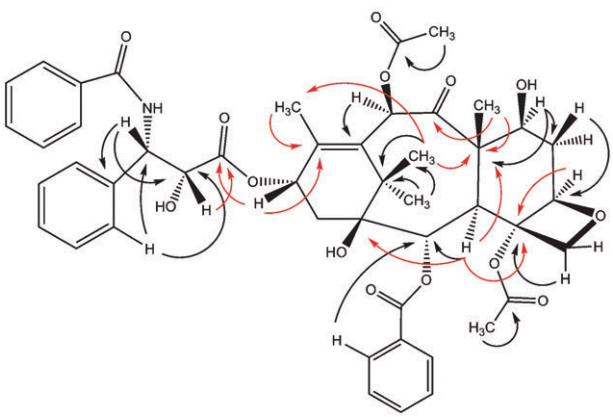

Fig. 4 The 28 ^{1}H to ^{13}C correlations that provide shift assignments in paclitaxel. The correlations shown in red provide assignment of 13 atoms to the asymmetric unit (*i.e.* **2a** or **2b**). The correlations in black provide assignment of shifts to specific molecular positions, but have poor resolution in either the ^{1}H or ^{13}C dimension and cannot provide assignments to the asymmetric unit. Insufficient ^{1}H and ^{13}C resolution at most aromatic positions prevents assignment of the ^{13}C atoms in the phenyl groups.

Table 1 Partial ^{13}C and ^{1}H shift assignments in solid paclitaxel

Position	δ ^{13}C/ppm	δ ^{1}H/ppm	Correlations $^{1}H \rightarrow {}^{13}C$[a]
1	79.1, 79.5	—	—
2	75.5	2.84	—
3	47.8, 48.4	2.13, 2.22	C3–H to C1, C2, C4 & C8
4	80.5, 82.9	—	—
5	84.8, 86.3	2.65, 2.43	C5–H to C4
6	37.2, 38.5	0.46, 0.78, 1.28, 1.53	C6–H to C5
7	73.8, 74.2	2.39, 2.34	C7–H to C6 & C8
8	58.6, 59.7	—	—
9	204.0, 206.0	—	—
10	76.3, 77.2	2.19, 2.22	C10–H to C11
11	132.6, 135.2	—	—
12	139.8, 144.3	—	—
13	70.5, 72.4	2.71, 2.82	C13–H to C1′ & C12
14	35.2, 36.6	1.03, 1.29, 1.18, 1.47	—
15	43.9	—	—
16	21.8, 23.0	0.70, 0.63	C16–H to C8, C15 & C18
17	26.2	−0.01	C17–H to C15 & C16
18	13.3, 14.1	1.03, 1.19	C18–H to C12
19	10.3, 11.5	1.03, 1.21	C19–H to C8 & C9
20	77.4	2.45 & 2.83	C20–H to C4
21	167.1, 168.1	—	—
23[b]	—	—	C23–H to C2 & C15
29	20.7, 21.6	1.45, 0.83	C29–H to C28
31	23.1, 23.2	1.19, 1.19	C31–H to C30
1′	170.7, 173.4	—	—
2′	71.5, 72.3	2.81, 2.63	C2′–H to C1′
3′	55.8	2.76	C3′–H to C2′ & C32
4′	165.5, 166.1	—	—
3′-*ipso*	142.1, 142.2	—	—
32[b]	—	—	C33–H to C2′ & C3′

[a] Assignments for C4′, C14 and C21 could not be clearly determined from the ^{1}H–^{13}C correlation data. Assignments were therefore made either by analogy to tensor principal values from 10-deacetyl baccatin III (carbons 14 and 21) or by the observation of a quadrupolar broadening from ^{14}N that varied with field strength (carbon 4′). [b] Assignments for carbons 2, 2′ and 3′-*ipso* were verified by a correlation to a nearby aromatic proton. However, the extensive degeneracy in the carbon spectrum prevented accurate determination of the carbon shifts for these aromatic carbons (C23 and C32).

Analysis of these data provided shift assignments to all molecular positions (Table 1) except phenyl sites due to dynamic behavior (discussed below) and severe isotropic overlap. At many nuclear positions, ^{13}C line doubling was observed in the 1D spectrum. At 13 of these sites (C1, C3, C4, C5, C8, C9, C12, C13, C16, C18, C19, C1′ & C2′) the ^{1}H lines were also found to be well resolved in the spectra. An example of the resolution typically achieved for these doubled lines is illustrated in Fig. 5 for carbons 18 & 19. This resolution allowed these 13 shifts to be assigned to a specific molecule of the asymmetric unit (Table 2). Admittedly, errors at this stage would render later structural conclusions irrelevant. Thus, assignments to the asymmetric unit were made only when both the ^{1}H and ^{13}C signals for all correlated signals were clearly resolved. Prior efforts to make such assignments using this conservative approach have been successful in all cases.[27] Assignments used herein are therefore considered to be correct.

The assignments of shifts to specific positions can be independently verified at certain sites by comparing the CSPVs with those previously reported for 10-deacetyl baccatin III where an X-ray structure was available.[34] NMR tensor data for **2** were acquired from prior studies[16] and are listed here in Table 3. In all cases a close match of CSPVs at corresponding positions in paclitaxel and 10-deacetyl baccatin III was found and verifies that the ^{1}H–^{13}C assignments reported here are correct (Table 3).

Computational modeling

Computer generated model structures were created from segments of the paclitaxel molecule (Fig. 3). Each model was selected in order to give accurate tensor values of nuclei in selected regions of paclitaxel. The rotation angle in the C10 acetyl group was established using model one. Model two was used to evaluate many of the C13 phenylisoserine sidechain conformations. This model constrains the **A** and **B** rings to conformations found in X-ray diffraction of **1a**. Inclusion of the **A** and **B** rings was found to be necessary for correct modeling at the C12 and C13 positions. Model two allowed determination of dihedral angles involving the C13–O, C1′–O, and C1′–C2′ bond axes. Model three was created in order to accurately explore the conformational features beyond the C3′ nuclei while still retaining an accurate representation of steric interactions within the C13 sidechain. This model contains the **A** ring and allows dihedral angles involving the C3′–C2′, O2–C2′, N–C3′, C4′–N, C3′*ipso*–C3′ and C4′*ipso*–C4′ bond axes to vary.

The systematic approach of a global conformational search of **2** was conducted by fixing the dihedral values of known structural features such as the tetracyclic ring system and performing a geometric optimization on the remaining molecular segments to obtain coordinates for shielding calculations. Shifts were calculated from computed shielding values

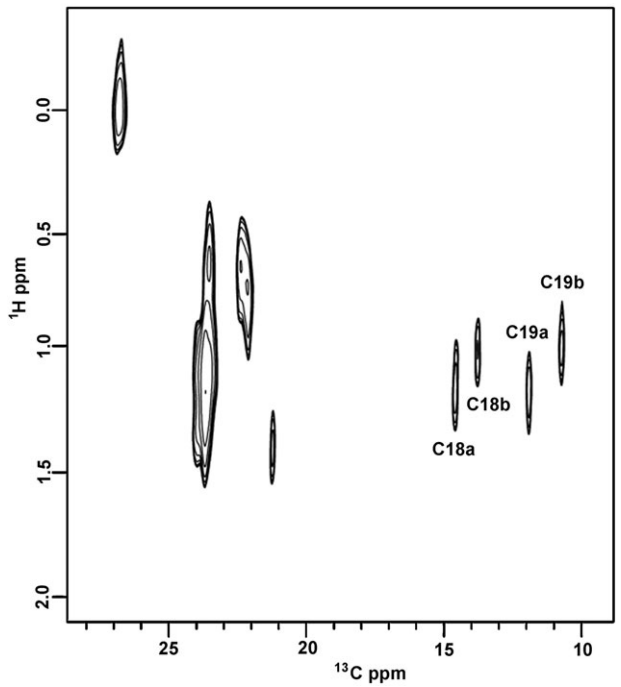

Fig. 5 An illustration of the resolution typically achieved in the ^{1}H–^{13}C HETCOR spectra of paclitaxel. The data shown were collected using a 130 μs cross polarization time. Positions C18 and C19 show the doubling of lines observed at many sites and the resolution in both the ^{1}H and ^{13}C dimensions needed to assign shifts to a specific molecule of the asymmetric unit.

(see the Experimental section), and these models were compared with experimental CSPVs at the relevent nuclei using an F-test.[50] F-Values for each predicted structure were obtained as $F = (d_i/d)^2$ where d_i represents the rms icosahedral distance of the ith conformer model from experiment, and d represents the model in the set which most closely matched experimental data. Inclusion of nuclei for the F-test was based on criteron described herein. The remaining torsion angles were examined by beginning at the rigid taxane core rotating the C13–O bond in 30.0° increments over the 360° range. At each point, the chosen angle was fixed and the remaining structure allowed to relax (*via* geometry optimization) before chemical shielding values were computed. The best-fit C13–O dihedral angle was retained (The F-test results of this rotation are shown in Fig. 6) and the process continued for the next flexible bond (*i.e.* O–C1′). This modeling was continued along the phenylisoserine sidechain until all conformational combinations had been explored and the overall best fit determined. In cases where a greater level of refinement was required, rotations of 10.0 or 15.0° were explored. The C10 acetyl conformation was established using a rigid model (model one) and sampling the dihedral angles about the C10–O bond axes in 30° increments.

After the most probable conformations were determined by this study, an additional computational model was constructed which, by combining model one and model three, simulated a major portion of the paclitaxel molecule. The baccatin core and the high-probability dihedral values listed in Table 6 were used as fixed values for each retained conformation and a geometry optimization was performed on the remaining structure. Theoretical chemical shift values were then computed for these structures to provide an overall comparison with experimental shift and to ascertain a simple ranking of retained conformers. The subsequent theoretical

Table 2 Assignments of ^{13}C shifts to the asymmetric unit in solid paclitaxel. Symbols *a*, *b* and *c* denote H/C correlations that were best observed at 130, 180 and 240 μs cross-polarization contact times, respectively

Position	Molecule A	Molecule B	Correlations ^{1}H → ^{13}C
1	79.5	79.1	—
3	48.4	47.8	C3–H to C1,[a] C4,[a] & C8[a]
4	82.9	80.5	—
5	84.8	86.3	C5–H to C4[a]
8	59.7	58.6	—
9	204.0	206.0	—
12	139.8	144.3	—
13	72.4	70.5	C13–H to C1′[c] & C12[c]
16	23.0	21.8	C16–H to C8[b] & C18[b]
18	14.1	13.3	C18–H to C12[c]
19	11.5	10.3	C19–H to C8[b] & C9[c]
1′	170.7	173.4	—
2′	72.3	71.5	C2′–H to C1′[b]

Table 3 Chemical shift principal values for carbon and nitrogen in paclitaxel **2**

	Paclitaxel conformer **2a**				Paclitaxel conformer **2b**			
Carbon no.	^{13}C δ_{iso}	δ_{11}	δ_{22}	δ_{33}	^{13}C δ_{iso}	δ_{11}	δ_{22}	δ_{33}
1[a]	*79.5*	94.3	84.3	60.0	*79.1*	94.5	83.5	58.9
2	*75.5*	96.6	80.4	49.6	*75.5*	96.6	80.4	49.6
3[a]	*48.4*	58.5	46.7	40.0	*47.8*	58.0	46.2	39.3
4[a]	*82.9*	98.9	92.8	56.9	*80.4*	95.6	90.3	55.6
5[a]	*84.8*	106.7	99.7	46.7	*86.3*	109.4	100.6	48.8
6	*37.2*	58.8	37.3	15.6	*38.5*	58.6	37.6	19.3
7	*73.8*	92.3	78.6	50.6	*74.2*	92.0	79.6	50.9
8[a]	*59.7*	80.7	53.2	45.1	*58.6*	78.8	52.2	44.9
9[a]	*204.0*	284.2	234.0	93.8	*206.0*	284.7	241.5	91.8
10	*76.3*	107.5	70.5	50.9	*77.2*	97.3	91.5	42.8
11	*132.6*	232.3	128.0	37.6	*135.2*	236.4	134.1	35.0
12[a]	*139.8*	238.1	139.7	41.6	*144.3*	243.9	147.2	41.9
13[a]	*72.4*	104.7	73.5	39.2	*70.5*	100.9	71.8	38.8
14	*35.2*	60.6	37.8	7.2	*36.6*	61.0	39.5	9.2
15	*43.9*	53.8	44.6	33.3	*43.9*	53.8	44.6	33.3
16[a]	*23.0*	38.5	24.1	6.4	*21.8*	37.7	22.7	5.2
17	*26.2*	49.3	31.5	−2.2	*26.2*	49.3	31.5	−2.2
18[a]	*14.1*	26.5	12.6	3.2	*13.3*	26.0	11.3	2.7
19[a]	*11.5*	20.1	11.5	2.7	*10.3*	19.1	9.4	2.3
20	*77.4*	110.6	71.6	49.6	*77.4*	110.6	71.6	49.6
21	*167.1*	253.0	135.0	113.4	*168.1*	252.7	139.2	112.4
22	*128.9*	221.1	144.6	20.9	*128.9*	221.1	144.6	20.9
28	*171.5*	262.7	139.1	111.9	*170.7*	262.1	137.5	112.4
29	*20.7*	37.4	29.5	−4.9	*21.6*	34.9	31.0	−1.0
31	*23.1*	41.4	31.2	−3.5	*23.2*	40.3	30.4	−1.1
1′[a]	*170.7*	262.1	137.5	112.4	*173.4*	265.5	137.4	117.5
2′[a]	*72.3*	85.2	79.4	52.2	*71.5*	89.1	65.7	59.8
3′	*55.8*	70.8	56.1	40.7	*55.8*	70.8	56.1	40.7
4′	*166.1*	242.5	160.7	95.1	*165.5*	241.1	163.1	92.3
4′*ipso*	*131.7*	221.2	143.7	30.1	*134.5*	224.4	152.8	26.3
3′*ipso*	*142.1*	238.1	170.6	17.7	*142.2*	230.2	172.0	24.5
N	*−254.4*	−155.7	−285.7	−321.9	*−267.8*	−177.7	−293.1	−332.6

[a] These sites were assigned to a specific molecule (**2a** or **2b**) of the asymmetric unit from ^{1}H–^{13}C heteronulcear correlation data as noted in Table 2. All other shifts were assigned to molecular positions but not to a particular molecule of the asymmetric unit. Isotropic shift values were obtained from a separate CPMAS spectrum and not derived from the FIREMAT data.

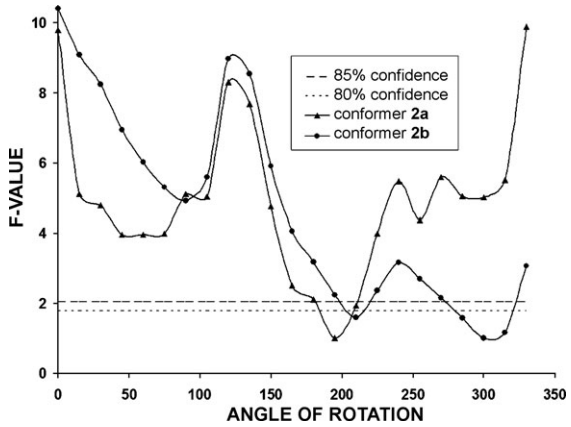

Fig. 6 F-Test of rms distances between CSPVs calculated for differing conformers of model two and experimental CSPVs of paclitaxel **2** at the nuclear positions C12, C13 and C1′ in evaluation of the dihedral C1′–O–C13–C12.

shift values were then plotted against experimental shifts and are given in Fig. 7.

Statistical methods

The extent to which chemical shift principal values of individual nuclei reflect conformational change is largely dependent upon its proximity to the region of variation. In principle, CSPV comparison at multiple nuclear locations would increase statistical accuracy. In practice, however, a balance must be reached that includes analysis of data from multiple nuclear sites to reduce ambiguity, yet restricts the total number of sites examined to eliminate positions that are too remote to reflect conformational changes.

A set of procedural guidelines was thus employed in selecting nuclei for comparison with computational models. First, there must be a peak assignment to the **a** or **b** conformer to ensure that the CSPVs being compared correspond to the correct molecule in the asymmetric unit. Next, those nuclei adjacent to or near the bonds forming rotation axes are preferred. Except in special cases such as π conjugation, where the electronic environment extends through conjugated bonds, the analysis was also limited to nuclei at the α, β and γ positions from the rotation axis. In particular, those nuclei that exhibited a strong conformational preference (*i.e.* those that have a large range in the rms distances between models and experimental CSPVs) gave more sensitive comparisons in the analysis. Finally, it was noted that when each model was optimized, an unusually large conformational variety was found in the remaining flexible portion of the molecule. The influence of this diversity diminishes with decreasing proximity to the nucleus in question and an effort was made to minimize this effect on the tensors. Thus, in addition to those nuclei which formed the bond axis of the dihedral under consideration, only CSPV information from nuclei in the rigid portion of any particular conformation was used (*i.e.* only those segments having their torsional angles fixed).

Conformer models were retained unless the F-value from CSPVs of at least three combined nuclear sites allowed their exclusion with at least 80% confidence. Previous conformational studies have shown this confidence level to be sufficient[18] and, in practice, most conformer models of paclitaxel were eliminated with a far greater statistical confidence than this modest value. An illustration of the selectivity obtained is given in Fig. 6 where the dihedral C1′–O–C13′–C12 is determined with high accuracy for both molecules in the asymmetric unit, **2a** and **2b**. Comparable accuracy is obtained at other positions. Due to the size of the grid search used in this study, this SSNMR approach yielded structures with dihedral errors of approximately ±15.0°. Dihedral values which could not be ascertained with this value are noted in Table 6.

While many studies have sorted conformational results by energy, gas phase calculated energies have questionable relevance to solids and may give a less reliable method of assessment unless experimental data such as SSNMR can be included. Such a combination may retain conformers that are not necessarily favorable in terms of energetics of an isolated molecule. This result can be partially understood by recalling that experimental NMR shifts are influenced by lattice structure. This may occur as a result of long range

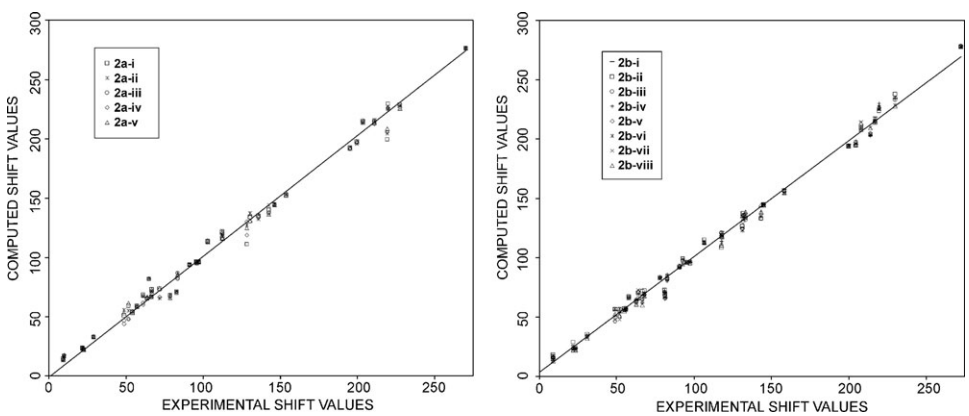

Fig. 7 Comparison between experimental CSPVs and the computed CSPVs of the best-fit model conformers at nuclear locations affected by the C13 sidechain and the C10 acetyl moiety. CSPVs for these graphs were calculated from a combination of model one and model three (Fig. 3) using the values obtained in this study for **2a** (left) and **2b** (right) given in Table 6. The additional substructures discussed in the section, ''An evaluation of intramolecular hydrogen bonding'' are omitted here but included in Fig. 8.

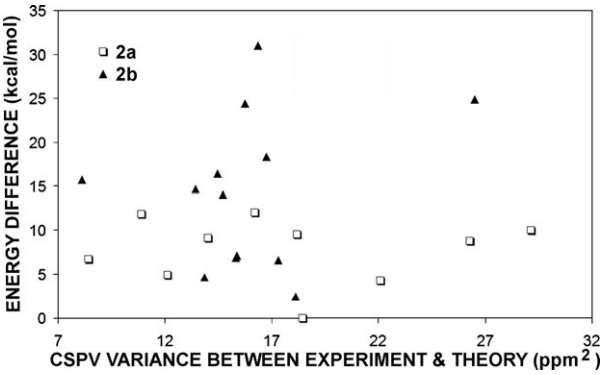

Fig. 8 Energy difference (in kcal mol^{-1}) *versus* CSPV variance (ppm^2) of paclitaxel **2a** and **2b** conformers retained with high statistical probability by this study. CSPVs examined were for the nuclear positions C13, C18, C1′, C2′ and C3′. This plot includes the alternate hydrogen bonding substructures discussed in the section, "An evaluation of intramolecular hydrogen bonding" and features the models wherein the dihedral angle C–C4′*ipso*-C4′═O was set at +45.0° (this study found a value of −45.0° to be an equally probable CSPV match). Here, CSPV fit and gas phase calculated energy values appear to be uncorrelated.

lattice effects or crowding by the lattice to give conformations not preferred in the gas phase. It is, therefore, not surprising that there are notable deviations between matches with NMR data and computed energies for isolated molecules. These deviations may be observed in the data of Fig. 8 wherein the relative energies for retained structures were plotted against the NMR fit (at positions affiliated with the phenylisoserine sidechain: C13, C18, C1′, C2′ and C3′). Energy differences were calculated relative to the structure with the lowest electronic energy (*i.e.* **2a-ii**). No correlation was found between energy and chemical shift ($R^2 = 2 \times 10^{-5}$ and $R^2 = 0.0538$ for **2a** and **2b**, respectively).

It is worthwhile to note that the spread of relative energies among the retained isomers is rather large. In some instances, the deviations observed are of such a magnitude that it would be tempting to give a lower probability ranking or to omit energetically unfavorable isomers. However, there remains significant uncertainty regarding contributions from lattice energy. Unless lattice energy can be included, it may be unwise to reject structures which give a suitable match to tensors. In future work, a more careful consideration of energy factors may be desirable.

Dynamic behavior in paclitaxel

Variable temperature analysis of **2** over a 170-°C range reveals that many of the aromatic carbons exhibit dynamic behavior in the solid (Fig. 9). Nevertheless, the observation of two ^{1}H–^{13}C dipolar correlations involving the phenyl ring at C3′ (Fig. 4) even at very short contact times (*e.g.* 70 μs) suggests that this ring is rigid. These results were confirmed in matches of NMR shift with computed conformers and the values may be viewed in Table 6. Prior work on 10-deacetyl baccatin III[34,51] has demonstrated that the benzoyl ring at C2 exhibits dynamic disorder involving oscillations of the phenyl ring about a two-fold rotation axis through C22 and C25. A comparison of the C21 tensors in paclitaxel with those in 10-deacetyl baccatin III shows a very close match of corresponding tensor values (σ = 2.7 ppm), implying that the benzoyl geometry in paclitaxel is very similar to that found in 10-deacetyl baccatin III. The C21 site is expected to be a sensitive indicator of phenyl ring orientation due to their close proximity and the fact that the C21═O moiety has π-electrons that delocalize into the ring. We, therefore, propose dynamic disorder in the benzoyl moiety of paclitaxel comparable to that found in 10-deacetyl baccatin III. Likewise, the phenyl group at C4′ is proposed to have dynamic disorder based on the fact that no ^{1}H–^{13}C correlations are found involving any of these phenyl sites. The CSPV data from C4′ best fit model structures with the phenyl ring rotated −45° or +45° from coplanarity with the C4′═O bond. These data suggest that the C4′ phenyl experiences stochastic jumps between these ±45° positions. The proposed structures displayed in Fig. 12 and 13 do not include these phenyl motions.

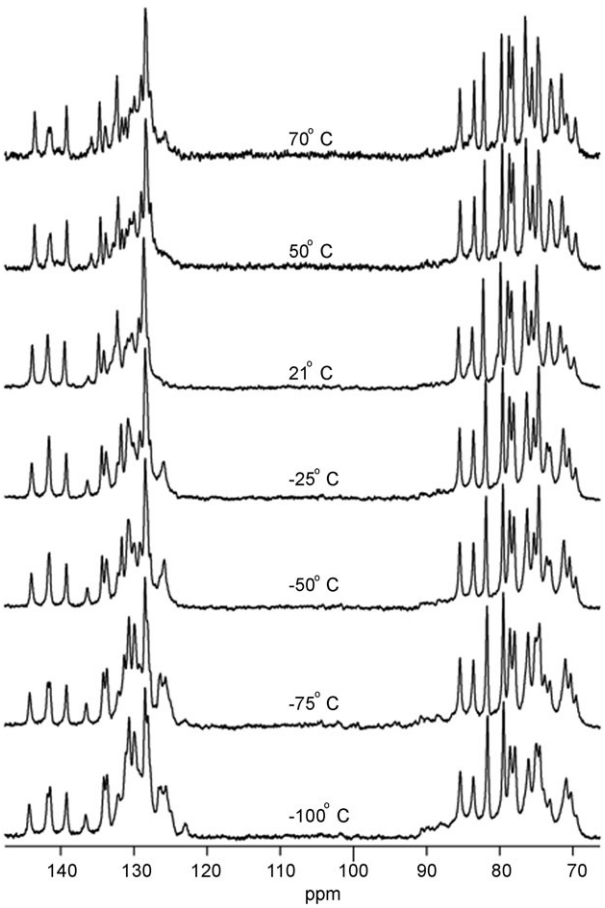

Fig. 9 The ^{13}C spectrum of paclitaxel over a 170-°C temperature range, emphasizing the aromatic carbons near 130 ppm. Significant changes with temperature are observed in the aromatic region indicating dynamic behaviour at these positions. This motion is proposed to occur primarily at the C4′ and C2 phenyls based on ^{1}H–^{13}C correlation data and ^{13}C tensor data. The C3′ phenyl appears to be static and likely gives rise to the aromatic lines observable at all temperatures. All other positions (*e.g.*, the region near 80 ppm) display less significant changes and therefore are considered to be nearly static.

Theoretical models were constructed to sample the energetic cost for this motion of the C4′ phenyl. These models, similar in

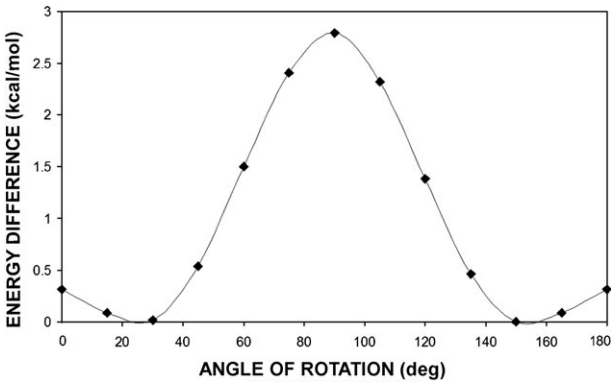

Fig. 10 Energy difference (in kcal mol^{-1}) between theoretical models constructed to sample the rotation about the dihedral C–C4′*ipso*–C4′═O.

composition to model three, sampled various degrees of tilt in the C4′ phenyl ring. Geometry optimized structures had electronic energies computed at the B3LYP 6-31 + G(2d,2p) level of theory and the results (displayed in Fig. 10) show the nature of this energy barrier. Here, the lowest energy conformation is reached when the dihedral C–C4′*ipso*-C4′═O is at 30.0°. This may seem to counter the intuitive sense that the ring should be planar with the C4′═O but when C–C4′*ipso*–C4′═O is at 0.0°, there is a repulsive interaction between at least one phenyl hydrogen and the N3′ hydrogen. This interaction likely dictates the overall conformation of the C4′ benzamide moiety.

CSPV comparison between *ab initio* conformers and paclitaxel

The *ab initio* conformation search utilized an array of more than 600 conformer models. Of these, most were eliminated through comparison with experimental values and only thirteen possessed a highly probable statistical match with experiment; five structures were retained as corresponding with the CSPVs of conformer **2a** (labelled **i** through **v** and shown in Fig. 12) and eight for conformer **2b** (labelled **i** through **viii** and displayed in Fig. 13). These structures (Table 6) could not be eliminated by comparison with chemical shift principle values and provided statistically-indistinguishable agreement with shift tensor data. The accuracy of CSPV matches for all thirteen computed structures is displayed in Fig. 7 as *ab initio* computed CSPVs *versus* experimental CSPVs for affected nuclei. Distances (rms) between computed CSPVs of those nuclei (correctly assigned to the asymmetric unit) affiliated with the sidechains at C10 and C13 and experimental data gave matches of 3.05 ppm (**2a-iii**) to 4.88 ppm (**2a-v**) for **2a** and 3.03 (**2b-iii**) to 5.19 ppm (**2b-ii**) for **2b**. A rudimentary ranking according to CSPV match at these same positions (C9, C12, C13, C18, C1′, C2′ and C3′) for **2a** and **2b** may be given. These are (from worst to best fit for C–C4′*ipso*–C4′═O at +45.0°) **2a-v** > **2a-i** > **2a-ii** > **2a-iv** > **2a-iii** and **2b-ii** > **2b-viii** > **2b-iv** > **2b-v** > **2b-i** > **2b-vi** > **2b-vii** > **2b-iii**.

The retained *ab initio* models for **2a** and **2b** conformers share many structural similarities with one another (Fig. 12 and 13). The most evident region of likeness between the two has already been established as the rigid baccatin core. Conformers **2a** and **2b** were also structurally similar to one another in the orientation of the phenylisoserine sidechain attachment at C13. Another region of likeness includes the conformation of the C10 acetyl group. The orientation of this later moiety (with the torsion angle defined as C30–O–C10–C9) was reflected in the CSPVs of nuclei C9, C10, C11, and C12 which differs in torsion angle from known conformers of paclitaxel by 122.0 to 165.0°[15] (Table 9).

Another similarity between **2a** and **2b**, already mentioned in the previous section (and in Table 6), is the equally-probable NMR fit for dihedral angles of ±45° at the C–C4′*ipso*–C4′═O torsion angle. Despite this CSPV match, the electronic energy of the model **2b-ii** with C–C4′*ipso*–C4′═O oriented at −45.0° is 13 kcal mol^{-1} greater than its counterpart at +45.0°. It is also 39 kcal mol^{-1} greater than the most energetically favorable model in the set (**2b-vii** with C–C4′*ipso*–C4′═O at −45.0°). This energetic difference is partially accounted for by a steric interaction between the hydrogens in C18 and at least one *ortho* phenyl-hydrogen in the ring at C4′ for the model **2b-ii** and emphasizes the risks of using energy data alone.

Of equal interest to the structural similarities between the best-fit conformers of **2a** and **2b** are the overall geometries of each. Conveniently, these conformations may be analyzed using perviously established definitions of known paclitaxel conformers (*i.e.* the polar, nonpolar and T-taxol forms).[6–14] In this comparison, it is of particular significance that the C13 sidechain conformation in the region spanning C13 to C3′ was established for **2** with high statistical confidence by the present study. This is a nontrivial result since the sidechain torsion angles involving C3′–C2′, C2′–C1′ and O–C13 bonds are primarily responsible for the orientation of the sidechain to the remainder of the paclitaxel structure.[9] This orientation, crucial in defining the structure–activity relationships of paclitaxel, provides a means to discuss **2a** and **2b** in terms of current definitions.

One feature frequently used to distinguish the differing conformers of paclitaxel is the relationship of the C13 sidechain to the tetracyclic baccatin core. In particular, the juxtaposition of the phenyl moieties in the C13 sidechain with the C2 benzoyl may be used to designate overall structure. This relationship may be quantified by the improper torsion angles[13] O–C2–C3′–N (ϕ_1) and O–C2–C3′–C(Ph) (ϕ_2) as shown in the Newman diagram of Fig. 11. These values are measured for conformers **2a** and **2b** and given in Table 4. Also shown are the radial distances between the benzoyl moiety at the C2 terminus and the pair of phenyl rings in the C13 sidechain ($\mathbf{r}_1$ and $\mathbf{r}_2$).

Evaluation of known conformers in terms of ϕ_1, ϕ_2, $\mathbf{r}_1$ and $\mathbf{r}_2$ provides approximate definitions for the polar and nonpolar forms. One feature of the polar conformation is that the angle ϕ_1 is negative and ϕ_2 is positive. Conversely, the nonpolar conformation is expected to have a positive value for ϕ_1 and a negative value for ϕ_2. The structure of T-taxol may therefore be considered to have nonpolar characteristics, as has been reported,[13,14] while both conformers in paclitaxel **1** share characteristics with the polar form. By this criterion, **2a-iii**, **2a-v**, **2b-v** and **2b-vi** correspond to the polar form while the remaining structures may be considered nonpolar.

It is apparent by the values of $\mathbf{r}_1$ and $\mathbf{r}_2$ for the models retained for **2a** and **2b** that hydrophobic collapse between the

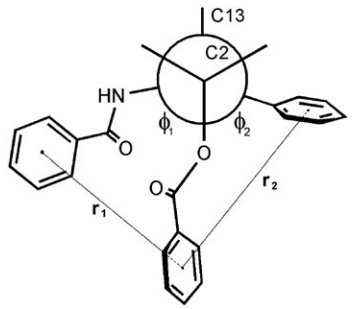

Fig. 11 Newman projection for paclitaxel conformation illustrating the improper torsion angles given by O–C2–C3′–N (ϕ_1) and O–C2–C3′–C(Ph) (ϕ_2) and ring-to-ring distances between the C2 benzoyl phenyl and the benzamido (C4′ phenyl) (r_1) and C3′ phenyl (r_2) centers, respectively.

Table 4 A comparison of improper torsion angles O–C2–C3′–N (ϕ_1) and O–C2–C3′–C(Ph) (ϕ_2) for the nonpolar and polar forms of paclitaxel (as summarized by Snyder *et al.*[13]), T-taxol,[13] the published structure of paclitaxel[15] **1**, and form **2** described herein. Ring-to-ring distances (in Å) between the C2 benzoyl phenyl and the benzamido (C4′ phenyl) (r_1) and C3′ phenyl (r_2) centers, respectively (Fig. 11)

	ϕ_1/deg	ϕ_2/deg	r_1/Å	r_2/Å
Nonpolar	42.0	−85.0	4.7	9.8
Polar	−52.0	28.0	11.6	5.7
T-Taxol	80.0	−58.0	9.4	10.0
1a	−51.1	65.0	13.3	9.9
1b	−57.1	25.8	5.3	11.4
2a-i	146.9	−83.2	12.1	11.3
2a-ii	165.6	−53.4	12.9	10.8
2a-iii	−104.9	42.4	14.0	9.4
2a-iv	117.9	−126.0	11.7	11.8
2a-v	−25.3	100.3	12.3	10.1
2b-i	172.9	−46.9	14.0	10.9
2b-ii	161.4	−48.1	12.7	9.9
2b-iii	−178.1	−48.1	14.5	11.0
2b-iv	−177.8	−48.4	11.7	10.9
2b-v	−56.5	71.7	13.0	10.7
2b-vi	−56.6	71.0	12.8	10.7
2b-vii	2.5	−153.9	9.3	11.9
2b-viii	−10.1	−179.0	9.3	12.1

C2 benzoyl moiety and the phenyl rings in the C13 phenylisoserine sidechain was not observed. In the instance of hydrophobic collapse, either $\mathbf{r}_1$ or $\mathbf{r}_2$ would be expected to be small (*i.e.* 3.0 to 6.0 Å). In the ring separations given herein for **2a** and **2b**, however, $\mathbf{r}_1$ ranges in values from 9.3 to 14.5 Å, while the range for $\mathbf{r}_2$ is 9.4 to 12.1 Å (Table 4). This is remarkably similar to the structural feature of T-taxol wherein ring-to-ring distances between these phenyl rings is nearly equidistant at 9.4 Å ($\mathbf{r}_1$) and 10 Å ($\mathbf{r}_2$).[13,14]

Table 5 Values of the H2′–C2′–C3′–H3′ dihedral for each of the retained conformer models of paclitaxel **2**. All dihedral angles are defined as in a Newman projection where the first atom listed is the proximal value and clockwise rotation is defined as positive

Structure	H–C2′–C3′–H (in degrees)	Form[a]
2a-i	38.1	Nonpolar
2a-ii	58.2	Nonpolar
2a-iii	150.3	Polar
2a-iv	1.9	—
2a-v	−144.4	—
2b-i	61.4	Nonpolar
2b-ii	61.0	Nonpolar
2b-iii	62.7	Nonpolar
2b-iv	61.5	Nonpolar
2b-v	−179.4	Polar
2b-vi	179.0	Polar
2b-vii	89.9	Nonpolar
2b-viii	87.0	Nonpolar

[a] The reference polar and nonpolar forms are defined to have H2′–C2′–C3′–H3′ dihedral angles of approximately 180.0 & 60.0°, respectively.

In addition to these characteristics of known paclitaxel conformers, another key feature distinguishing the polar conformation from the nonpolar form (as described by Ojima *et al.*[8]) is the measurement of the dihedral given by H2′–C2′–C3′–H3′ with the value for the polar form at 180.0° and the nonpolar at 60.0°. For the structures retained for paclitaxel **2a** and **2b** these measurements are given in Table 5.

Of the thirteen structures, four (**2a-iii**, **2b-v** and **2b-vi**) may be classified in this manner as polar, eight (**2a-i**, **2a-ii**, **2b-i**, **2b-ii**, **2b-iii**, **2b-iv**, **2b-vii** and **2b-viii**) may be categorized as nonplar, and two (**2a-iv** and **2a-v**) have a dihedral value that does not come within a 30° range of either form. It is interesting to note that those structures considered polar by this analysis included those forms also determined to be polar by evaluation of the improper torsion angles ϕ_1 and ϕ_2 (Table 4).

Table 6 lists key dihedral measurements for the five structures of conformer **2a** and the eight structures of conformer **2b**. Of particular interest for **2a** is that conformational diversity is found only in dihedral angles involving rotation about the C3′–C2′ and N–C3′ bonds. At all other positions, the structures for **2a** tend to be conformationally similar to one another. The less reliable gas phase energy assessment ranks

Table 6 Dihedral values (in degrees) for model conformers matching experimental CSPVs of paclitaxel structures **2a** and **2b**. All dihedral angles are defined as in a Newman projection where the first atom listed is the proximal value and clockwise rotation is defined as positive. The symbols **a**, **b** and **c** denote errors of ±20.0, ±30.0 and ±45.0°, respectively, in the predicted angle. All other dihedral angles have an error of ±15.0° or less

Torsion angle	**2a-i**	**2a-ii**	**2a-iii**	**2a-iv**	**2a-v**	**2b-i**	**2b-ii**	**2b-iii**	**2b-iv**	**2b-v**	**2b-vi**	**2b-vii**	**2b-viii**
C30–O–C10–C9	−45.0	−45.0	−45.0	−45.0	−45.0	−60.0	−60.0	−60.0	−60.0	−60.0	−60.0	−60.0	−60.0
C1′–O–C13–C12	−165.0	−165.0	−165.0	−165.0	−165.0	−60.0	−60.0	−60.0	−60.0	−60.0	−60.0	−150.0	−150.0
C2′–C1′–O–C13	180.0	180.0	180.0	180.0	180.0	150.0	150.0	150.0	150.0	150.0	150.0	180.0	180.0
O–C2′–C1′═O	180.0[b]	180.0[b]	180.0[b]	180.0[b]	180.0[b]	105.0	105.0	105.0	105.0	105.0	105.0	−15.0[c]	−15.0[c]
N–C3′–C2′–C1′	30.0	60.0	150.0	0.0	210.0	60.0	60.0	60.0	60.0	180.0	180.0	90.0	90.0
C4′–N–C3′–C2′	60.0	−15.0	−120.0	−120.0	−120.0	0.0	0.0	−105.0	−105.0	−105.0	−105.0	−135.0	−135.0
O═C4′–N–C3′	15.0	15.0	15.0	15.0	15.0	15.0[a]	−170.0	15.0[a]	−170.0	15.0[a]	−170.0	15.0[a]	−170.0
C–C3′*ipso*–C3′–C2′	−75.0	−75.0	−75.0	−75.0	−75.0	−60.0[b]	−60.0[b]	−60.0[b]	−60.0[b]	−60.0[b]	−60.0[b]	−60.0[b]	−60.0[b]
C–C4′*ipso*–C4′═O	±45.0	±45.0	±45.0	±45.0	±45.0	±45.0	±45.0	±45.0	±45.0	±45.0	±45.0	±45.0	±45.0

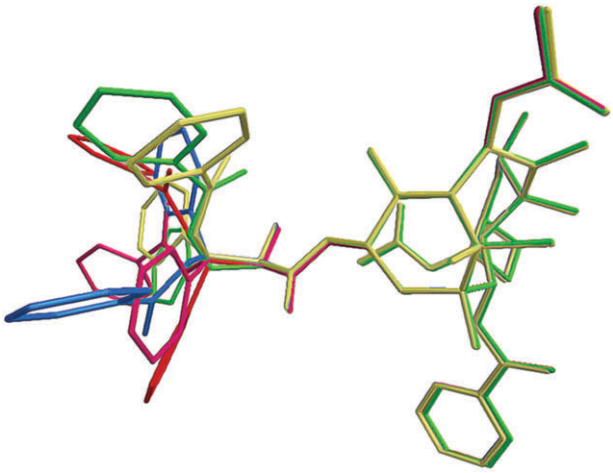

Fig. 12 Five conformer models providing high probability matches to the experimental CSPVs of paclitaxel **2a**. This overlay features a C–C4′*ipso*–C4′═O dihedral angle of −45.0°, but +45.0° is equally probable.

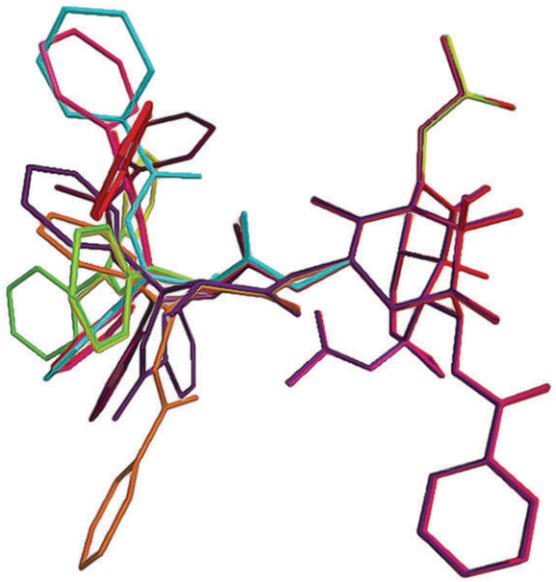

Fig. 13 Eight conformer models providing probable matches to the experimental CSPVs of paclitaxel **2b**. The above models display C–C4′*ipso*–C4′═O angle of −45.0° while +45.0° provides an equally-probable solution.

model **2a-ii** as the most energetically likely among conformers retained for **2a**. The energy difference between the remaining four models and **2a-ii** ranges between 4.3 and 12.0 kcal mol^{-1}. The overlay in Fig. 12 demonstrates the conformational similarity in the five models retained for **2a**.

Conformer **2b** had more matches with model structures than for **2a**. An evaluation of the computed energy of the final structures show that **2b-vii** is the lowest energy. Four of the remaining structures were energetically unfavorable and all possess the dihedral O═C4′–N–C3′ = −170.0° (**2b-ii**, **2b-iv**, **2b-vi** and **2b-viii**). These unfavored structures differ in energy from **2b-vii** by 10.95–39.27 kcal mol^{-1}. In contrast, the structures **2b-i**, **2b-iii** and **2b-v** feature the dihedral O═C4′–N–C3′ = 15.0° and generally have energies close to **2b-vii** (3.15 to 11.9 kcal mol^{-1} different). However, it is unlikely that the O═C4′–N–C3′ dihedral is the sole source of the energy differences since model **2b-viii** differs from **2b-vii** only at the O═C4′–N–C3′ dihedral angle, yet is energetically similar to **2b-vii**.

It is of interest that several of the **2b** structures share conformational features with the T-taxol conformation. As mentioned previously, like T-taxol, they have extended C13 sidechain moieties and most have nonpolar characteristics with the C4″–benzamidophenyl shifted significantly away from the C2 benzoyl center.[14] Additionally, the mechanism by which T-taxol is said to bind to microtubules is related to the location of β-tubulin's His-227 in the taxoid binding pocket created by the space between the C2 benzoyl and C4′ benzamide. Therefore, the methyl hydrogens from the acetyl at C4 in T-taxol and the *o*- and *m*-hydrogens of the C3′ phenyl are close (2.5–2.9 and 4.3–4.9 Å, respectively).[14] These distances are similar to the range reported for four of the eight structures for **2b** (**2b-i**, **2b-ii**, **2b-iii**, and **2b-iv**) and are shown in Table 7 and Fig. 14 along with these values for all probable conformers.

Ambiguity in conformational assignment of paclitaxel was limited to the C3′ sidechain moieties. Conformational uncertainty here was due to the quadrupolar coupling of the ^{14}N to the C3′ and C4′ nuclei, which split these carbon resonances. The resultant larger error in chemical shift tensor values at these locations prevented unique conformational assignment. While the nitrogen CSPVs were extremely sensitive to conformation, there was no experimental assignment of nitrogen shift to a specific molecule of the asymmetric unit. A statistical match of nitrogen shifts with computed CSPVs of models with partially solved features of **2a** and **2b** in a method already described[18] revealed a probable assignment and these values are listed (Table 3).

An evaluation of intramolecular hydrogen bonding

In the present structural analysis, the differences in CSPVs have been attributed primarily to differences in molecular conformation in structures **2a** and **2b**. However, hydrogen bonding can also have a significant influence at certain positions such as N3′[52] and carbons doubly bonded to oxygen.[53] The approach used herein provides information regarding

Table 7 H–H separations (in Å) between the C4 acetate methyl group and the *ortho*- and *meta*- positions of the C3′ phenyl ring and the C4′ benzamide. Comparison is to "T-taxol" conformer values. Instances where the values are unavailable are indicated by an asterisk (*)

	T-Taxol	**2a-i**	**2a-ii**	**2a-iii**	**2a-iv**	**2a-v**	**2b-i**	**2b-ii**	**2b-iii**	**2b-iv**	**2b-v**	**2b-vi**	**2b-vii**	**2b-viii**
C4′*o*–C4	*	6.4	6.7	5.7	7.1	5.7	7.8	5.9	7.3	6.6	4.4	5.4	4.3	3
C4′*m*–C4	*	8.7	9.2	8.0	9.6	8.0	10.2	6.7	9.7	7.8	6.5	6.8	6.6	2.8
C3′*o*–C4	2.5–2.9	4.8	4.7	5.0	5.2	5.7	4.0	3.7	3.8	3.8	4.1	4.1	4.1	4.8
C3′*m*–C4	4.3–4.9	6.4	6.2	7.0	6.7	7.9	5.2	4.6	4.7	4.7	6.2	6.2	6.4	7.3

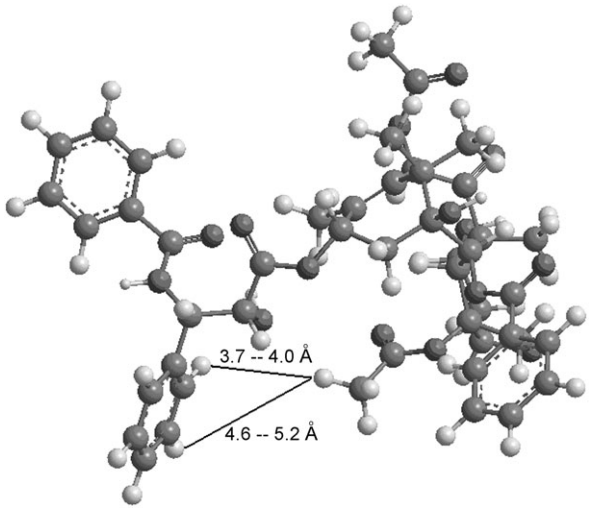

Fig. 14 The observed range for H–H separations between the C4 acetate methyl protons and the *ortho* and *meta* H's of the C3′ phenyl ring in models **2b-i**, **2b-ii**, **2b-iii** and **2b-iv**. The model shown in this figure is **2b-i**.

intramolecular hydrogen bonding, since O···O and O···N distances are provided from the retained model structures. A visual assessment of these structures allows feasible hydrogen bonds to be determined at a given site. In certain structures more than 1 bonding arrangement is possible. Indeed, by exploring all possible placements of the 2′ OH donor hydrogen, 8 of the 13 structures were found to have 2 alternative hydrogen bonding arrangements. Structure **2a-v**, in fact, has a conformation that allows for 3 alternative hydrogen bonded structures involving the 2′ OH. In these cases, many of the alternative structures appear to be equally favorable in terms of O–H···X (X = O or N) geometry. All these new structures were statistically indistinguishable from their parent structures based on a comparison of tensor values at positions C1′, C2′, C3′ and C13. One structure (**2b-vii2**) possessed an electronic energy that was 1.35 kcal mol^{-1} lower than the previously obtained low energy value for the set (**2b**). Thus, a total of 24 structures were ultimately retained: 13 obtained from the prior analysis and 11 differing primarily in placement of the 2′ OH proton from one of the original 13. These 11 new substructures retain most of the conformational features of their parent structures and are, therefore, denoted in terms of these structures (*i.e.* **2a-i2**, **2a-iii2**, **2a-iv2**, **2a-v2**, **2a-v3**, **2b-i2**, **2b-ii2**, **2b-iii2**, **2b-vi2**, **2b-vii2** and **2b-iii2**). The CSPV variances and electronic energies for these structures are included among the data shown in Fig. 8.

All 24 of the retained structures of paclitaxel have at least 1 intramolecular hydrogen bond (Table 8). Structure **2a-i** with 3 internal bonds has the most extensive intramolecular hydrogen bonding, while 12 structures (**2a-iii**, **2a-iv**, **2a-v**, **2b-iii**, **2b-iv**, **2b-v**, **2b-vi**, **2a-i2**, **2a-iii2**, **2a-iv2**, **2a-v3** and **2b-i2**) have only one such bond. The O2′–H···O13 hydrogen bond is observed in the majority of the structures (16 out of 24) and the H at O2′ acts as a hydrogen bond donor in 84.4% of the bonds observed. The extensive occurrence of the 2′ OH hydrogen in internal hydrogen bonding demonstrates that it is optimally situated to form intramolecular bonds in paclitaxel and implies that it will be less likely to form hydrogen bonds to microtubules. This is because OH groups that act as intramolecular hydrogen bond donors tend to be much less available for intermolecular hydrogen bonding.[55] This comparison also allows conjecture regarding the difference between **2a** and **2b**. It is observed that the O2′–H···O1′ interaction is exclusive to structure **2b**, occurring in nearly half of the structures. Likewise, the O2′–H ···O4′ pairing occurs primarily in **2a**. Thus, one explanation of the differences between **2a** and **2b** is that the 2′ OH is used as a donor to O1′ in **2b** and as a donor to O4′ in **2a**. However, since these differences are not found in all structures, it cannot be unambiguously proposed as the sole explanation.

Comparison of paclitaxel 2 with 1 and related analogs

As a final observation, it is interesting to contrast the conformational differences between paclitaxel **2** obtained entirely from matches with CSPVs (Table 6) with those analogs of paclitaxel which have known X-ray structures. The following paclitaxel analogs were therefore used as a basis for comparison with the results given here for paclitaxel **2**: docetaxel[56] (taxotere) **3**, 10-deacetyl-7-epitaxol[57] **4a** and **4b**, 7-mesylpaclitaxel[33] **5**, taxine A acetone solvate[54] **6**, and 2′,3′-*O*,*N*-isopropylidene-7-*O*-(triethylsilyl) paclitaxel[58] **7**.

Of these structures, **3**, **4a** and **4b** are hydrophobically collapsed and **5** shares features with both the polar and nonpolar conformations. Molecular conformations obtained from the crystal structures of these analogs are illustrated in Fig. 15 with dihedral values given in Table 9. These values may be contrasted with Table 6 which contains corresponding values determined by this study for structure **2**.

An interesting difference between these analogs of paclitaxel and conformers **2a** and **2b** is in the dihedral angle of the C10 acetyl. Conformers **2a** and **2b** share the dihedral value C30–O–C10–C9 = 300.0°. This differs by 122.0 and 165.0° from values measured for known crystal structures.

Table 8 Summary of hydrogen bonding parameters in the 13 best-fit structures of paclitaxel

D–H···A	D–H (Å)	H···A (Å)	D···A (Å)	D–H···A (°)	Occurrence
N3′–H···O1′	0.97	2.9	3.06	89.8	**2a-i**
N3′–H···O2′	1.0	2.36–2.85	2.72–2.93	84.8–102.11	**2b-vii**, **2b-vii2**, **2b-viii**, **2b-viii2**
O2′–H···N3′	0.97	2.70–3.12	3.05–3.33	86.8–101.7	**2b-ii**, **2b-iii2**
O2′–H···O1′	0.97	2.17–3.25	2.67–3.34	86.12–111.7	**2b-i**, **2b-ii**, **2b-vii**, **2b-viii**, **2b-vi2**
O2′–H···O4′	0.97	1.97–3.00	2.74–3.7	130.0–142.7	**2a-i**, **2a-ii**, **2a-v2**, **2b-i**
O2′–H···O13	0.97	2.22–2.78	2.52 – 2.99	84.3–101.7	**2a-i**, **2a-ii**, **2a-iii**, **2a-iv**, **2a-v**, **2b-iii**, **2b-iv**, **2b-v**, **2b-vi**, **2a-vi2**, **2a-iii2**, **2a-iv2**, **2a-v3**, **2b-i2**, **2b-vii2**, **2b-viii2**

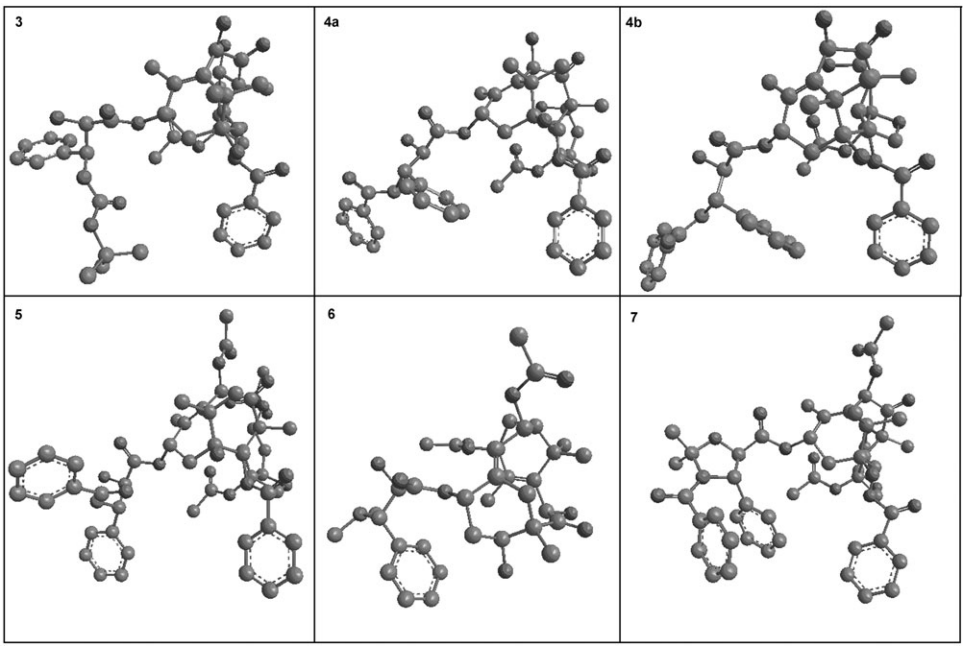

Fig. 15 Paclitaxel analogs determined by previous X-ray studies are given as a basis of comparison with paclitaxel conformers determined by this study. The conformers are docetaxel (taxotere) **3**[56] and 10-deacetyl-7-epitaxol **4a** and **4b**.[57] These display the hydrophobically collapsed conformation of paclitaxel. 7-Mesylpaclitaxel **5**[33] shares conformational features with both the nonpolar and polar forms. Also shown is taxine A acetone solvate[54] **6** and 2′,3′-*O*,*N*-isopropylidene-7-*O*-(triethylsilyl) paclitaxel **7**.[58]

Table 9 Selected torsion angles for paclitaxel and its analogs where **2** is the paclitaxel molecule assigned herein. All dihedral angles are defined as in a Newman projection where the first atom listed is the proximal value and clockwise rotation is defined as positive. Since all analogs do not include every stereochemical feature of paclitaxel, certain torsion angles are unavailable for comparison; these are marked with an asterisk (*)

Torsion angle	**1a**	**1b**	**3**	**4a**	**4b**	**5**	**6**	**7**
C30–O–C10–C9	95.4	89.1	—*	—*	—*	76.3	—*	105.1
C1′–O–C13–C12	−92.1	−100.9	−101.0	−111.1	−102.8	−99.5	—*	−93.1
C2′–C1′–O–C13	179.8	−176.9	168.0	−176.5	−166.4	−166.4	−166.1	−158.0
O–C2′–C1′═O	93.3	41.1	-2.2	55.9	46.7	21.7	46.4	16.8
N–C3′–C2′–C1′	176.0	178.6	56.5	−176.3	168.7	61.4	164.4	135.1
C4′–N–C3′–C2′	−117.8	−155.2	−141.4	−109.2	−143.1	−98.6	67.1	174.1
O═C4′–N–C3′	1.3	−0.9	12.9	−6.3	−3.8	1.5	—*	−179.0
C–C3′*ipso*-C3′–C2′	166.6	102.4	83.6	133.8	107.5	118.1	135.4	115.0
C–C4′*ipso*-C4′═O	28.4	−3.1	—*	29.7	−38.7	30.0	—*	71.1

Attachment of the C13 sidechain also showed between 30.0 and 95.0° difference between the C1′–O–C13–C12 dihedral angle in **2a** and **2b** and the crystal structure paclitaxel analogs. Experimental agreement with paclitaxel analogs for the C2′–C1′–O–C13 torsion angle is found in this study and torsion around the C2′–C1′ for **2b** agrees with certain X-ray values within the margin of error. Values for the C3′–C2′–C1′–O dihedral in **2a** are unprecedented, however, giving torsion angles at least 90.0° different from these analogs. Similarly, **2a** finds only partial agreement with these X-ray analogs in dihedral angles around the C3′–C2′ bond. In contrast, **2b** matched known analogs at the dihedral involving the C3′–C2′ bond axis.

Conclusions

The high-probability assignment of structure in paclitaxel has been demonstrated using CSPV data at multiple nuclear locations in conjunction with model conformers. These models required only fragments of the paclitaxel structure due to the fact that CSPVs are dominated by the local molecular environment.

Assignment of chemical shift to the correct molecule in the asymmetric unit (**a** or **b**) is achieved through the use of a heteronuclear correlation technique and makes possible the analysis of CSPVs at multiple sites. Of the over 600 paclitaxel conformational models analyzed, fewer than 5% were found to match experiment.

The structures retained for **2a** and **2b** have varying similarities to the polar and nonpolar forms, although all possessed extended C13 sidechain conformations. Furthermore, half of the models retained for **2b** showed striking similarities to the conformation known as T-taxol, a structure elucidated from electron crystallography models and reported to be highly bioactive. To date, no diffraction structure has been reported for this conformer.

This analysis of paclitaxel is the first complete conformational characterization by SSNMR for which $Z' > 1$.[27,48] Prior analyses have only discovered fragments rather than complete structure.

While the approach described is computationally-intensive, it has the advantage of searching the complete conformational space for heavier atoms. Thus, successful execution of the CSPV comparison reduces the chance of becoming trapped in local minima and provides structures that are difficult to determine by other methods. It must be emphasized that accuracy in this approach is strongly dependent on correct assignment of experimental shifts and the availability of measured principal values.

The structures proposed in this study represent favorable conformations of paclitaxel and add to the information already available from solution analysis and other studies. Taken together, these data help define the conformational space available to paclitaxel.

Acknowledgements

Funding for this project was provided by the National Institute of Health under grant 5R01GM08521-44. We gratefully acknowledge Donald Mastropaolo and the late Arthur Camerman for providing coordinates for the single crystal polymorph of paclitaxel (**1a** and **1b**). We wish to thank Roland Franke and Natural Pharmaceuticals Inc. for supplying the sample of paclitaxel upon which this study was based. We thank Dewey H. Barich for collection and analysis of the FIREMAT data on paclitaxel **2**. We also thank Eduardo M. Reyes-Vargas and Emily C. Heider for providing helpful insights during this research.

References

1 C. M. Spencer and D. Faulds, *Drugs*, 1994, **48**(5), 794–847. Review: cancers treated by paclitaxel include advanced squamous cell carcinoma of the head and neck, malignant melanoma, advanced non-small cell lung cancer (NSCLC), small cell lung cancer (SCLC), germ cell cancer, urothelial cancer, oesophageal cancer, non-Hodgkin's lymphoma or multiple myeloma, and was successfully combined with cisplatin, carboplatin and/or etoposide in patients with NSCLC, SCLC or advanced squamous cell carcinoma of the head and neck.

2 M. A. Jordan, *Curr. Med. Chem.: Anti-Cancer Agents*, 2002, **2**, 1–17.

3 E. J. Rowinsky and R. C. Donehower, *New Engl. J. Med.*, 1995, **333**(1), 75.

4 (*a*) D. I. Axel, W. Kunert, C. Goggelmann, M. Oberhoff, C. Herdeg, A. Kuttner, D. H. Wild, B. R. Brehm, R. Riessen, G. Koveker and K. R. Karsch, *Am. Heart Assoc.*, 1997, **96**, 636–645; (*b*) B. Scheller, C. Hehrlein, W. Bocksch, W. Rutsch, D. Haghi, U. Dietz, M. Bohm and U. Speck, *New Engl. J. Med.*, 2006, **355**(20), 2113–2124.

5 (*a*) L. R. Wiseman and C. M. Spencer, *Drugs Aging*, 1998, **12**(4), 305–334; (*b*) L. J. Scott and D. P. Figgitt, *CNS Drugs*, 2004, **18**(6), 379–396 (review); (*c*) C. Forbes, L. Shirran, A. M. Bagnall, S. Duffy and G. Ter Riet, *Health Technol. Assess.*, 2001, **5**(28), 1–110 (review); (*d*) G. L. Plosker and M. Hurst, *Pharmacoeconomics*, 2001, **19**(11), 1111–1134 (review).

6 J. Dubois, D. Guenard, F. Guerette-Voegelein, N. Guedira, P. Potier, B. Gillet and J.-C. Beloeil, *Tetrahedron*, 1993, **49**, 6533–6544.

7 H. J. Williams, A. I. Scott, R. A. Dieden, C. S. Swindell, L. E. Chirlian, M. M. Francl, J. M. Heerding and N. E. Krauss, *Can. J. Chem.*, 1994, **72**, 252–260.

8 I. Ojima, S. D. Kuduk, S. Chakravarty, M. Ourevitch and J.-P. Begue, *J. Am. Chem. Soc.*, 1997, **119**, 5519–5527.

9 (*a*) H. J. Williams, A. I. Scott, R. A. Dieden, C. S. Swindell, L. E. Chirlian, M. M. Francl, J. M. Heerding and N. E. Krauss, *Tetrahedron*, 1993, **49**, 6545–6560; (*b*) D. G. Vander Velde, G. I. Georg, C. G. Grunewald, W. Gunn and L. A. Mitscher, *J. Am. Chem. Soc.*, 1993, **115**, 11650–11651.

10 I. Ojima, S. Chakravarty, I. Tadashi, S. Lin, L. He, S. B. Horowitz, S. D. Kuduk and S. J. Danishefsky, *Proc. Natl. Acad. Sci. U. S. A.*, 1999, **96**, 4256–4261.

11 J. Jimenez-Barbero, F. Amat-Guerri and J. P. Snyder, *Curr. Med. Chem.: Anti-Cancer Agents*, 2002, **2**, 91–122.

12 Y. Li, B. Poliks, L. Cegelski, M. Poliks, Z. Gryczynski, G. Piszcsek, P. G. Jagtap, D. R. Studelska, D. G. I. Kingston, J. Schaefer and S. Bane, *Biochemistry*, 2000, **39**, 281–291.

13 J. P. Snyder, J. H. Nettles, B. Cornett, K. H. Downing and E. Nogales, *Proc. Natl. Acad. Sci. U. S. A.*, 2001, **98**, 5312–5316.

14 T. Ganesh, R. C. Guza, S. Bane, R. Ravindra, N. Shanker, A. S. Lakdawala, J. P. Snyder and D. G. I. Kingston, *Proc. Natl. Acad. Sci. U. S. A.*, 2004, **101**(27), 10006–10011.

15 D. Mastropaolo, A. Camerman, Y. Luo and G. D. Brayer, *Proc. Natl. Acad. Sci. U. S. A.*, 1995, **92**, 6920–6924. We acknowledge Donald Mastropaolo and Arthur Camerman for providing the coordinates.

16 J. K. Harper, D. H. Barich, E. M. Heider, D. M. Grant, R. R. Franke, J. H. Johnson, Y. Zhang, P. L. Lee, R. B. Von Dreele, B. Scott, D. Williams and G. B. Ansell, *Cryst. Growth Des.*, 2005, **5**(5), 1737–1742.

17 (*a*) Z. Gu and A. E. McDermott, *J. Am. Chem. Soc.*, 1993, **115**, 4282–4285; (*b*) Z. Gu, R. Zambrano and A. E. McDermott, *J. Am. Chem. Soc.*, 1994, **116**, 6368–6372; (*c*) Y. Wei, A. C. de Dios and A. E. McDermott, *J. Am. Chem. Soc.*, 1999, **121**, 10389–10394; (*d*) D. H. Barich, J. S. Clawson, D. Stueber, M. Strohmeier, R. J. Pugmire and D. M. Grant, *J. Phys. Chem. A*, 2002, **106**, 11375–11379.

18 J. K. Harper, A. E. Mulgrew, J. Y. Li, D. H. Barich, G. A. Strobel and D. M. Grant, *J. Am. Chem. Soc.*, 2001, **123**, 9837–9842.

19 (*a*) Representative studies include: J. C. Facelli and D. M. Grant, *Nature*, 1993, **365**(6444), 325–327; (*b*) E. Oldfield, *J. Biomol. NMR*, 1995, **5**(3), 217–225; (*c*) D. M. Grant, F. Liu, R. J. Iuliucci, C. G. Phung, J. C. Facelli and D. W. Alderman, *Acta Crystallogr., Sect. B*, 1995, **51**(4), 540–546; (*d*) S. Ghelli, G. Rastelli, D. Barlocco, M. Rinaldi, D. Tondi, P. Pecorari and M. P. Costi, *Bioorg. Med. Chem.*, 1996, **4**(10), 1783–1794; (*e*) R. D. Berger and P. H. Bolton, *J. Biomol. NMR*, 1997, **10**(2), 129–142.

20 (*a*) A. Soderquist, J. C. Facelli, W. J. Horton and D. M. Grant, *J. Am. Chem. Soc.*, 1995, **117**, 8441–8446; (*b*) J. K. Harper, G. McGeorge and D. M. Grant, *J. Am. Chem. Soc.*, 1999, **121**, 6488–6496.

21 (*a*) D. Stueber, F. N. Guenneau and D. M. Grant, *J. Chem. Phys.*, 2001, **114**, 9236–9243; (*b*) A. C. deDios and E. Oldfield, *Chem. Phys. Lett.*, 1993, **205**, 108–116; (*c*) A. C. deDios, D. D. Laws and E. Oldfield, *J. Am. Chem. Soc.*, 1994, **116**, 7784–7786; (*d*) M. B. Ferraro, V. Repetto and J. C. Facelli, *NMR Solid State*, 1998, **10**, 185–189.

22 D. M. Grant, in *Encyclopedia of NMR*, ed. D. M. Grant and R. K. Harris, Wiley, Chichester, 1996, vol. 2, pp. 1298–1321.

23 J. K. Harper, D. H. Barich, J. Z. Hu, G. A. Strobel and D. M. Grant, *J. Org. Chem.*, 2003, **68**, 4609–4614.

24 (*a*) J. Heller, D. D. Laws, M. Thomaselli, D. S. King, D. E. Wemmer, A. Pines, R. H. Havlin and E. Oldfield, *J. Am. Chem. Soc.*, 1997, **119**, 7827–7831; (*b*) H. Le, J. G. Pearson, A. C. de Dios and E. Oldfield, *J. Am. Chem. Soc.*, 1995, **117**, 3800–3807; (*c*) R. H. Havlin, H. Le, D. D. Laws, A. C. de Dios and E. Oldfield, *J. Am. Chem. Soc.*, 1997, **119**, 11951–11951.

25 (*a*) C. M. Rienstra, L. Tucker-Kellogg, C. P. Jaroniec, M. Hohwy, B. Reif, M. T. McMahon, B. Tidor, T. Lozano-Perez and R. G. Griffin, *Proc. Natl. Acad. Sci. U. S. A.*, 2002, **99**(16), 10260–10265; (*b*) C. P. Jaroni, C. E. MacPhee, V. S. Bajaj, M. T. McMahon, C. M. Dobson and R. G. Griffin, *Proc. Natl. Acad. Sci. U. S. A.*, 2003, **101**, 711–716.

26 (*a*) B. Elena, G. Pintacuda, N. Mifsud and L. Emsley, *J. Am. Chem. Soc.*, 2006, **128**, 9555–9560; (*b*) F. Castellani, B.-J. van Rossum, A. Diehl, M. Schubert and H. Oschkinat, *Nature*, 2002, **420**, 98–102.

27 J. K. Harper, M. Strohmeier and D. M. Grant, *J. Magn. Res*., in press.
28 (*a*) A. C. Scheiner, J. Baker and J. M. J. Aldzelm, *Comput. Chem*., 1997, **18**, 775; (*b*) W. J. Hehre, *Practical Strategies for Electronic Structure Calculations: Wavefunction*, 1995.
29 (*a*) A. A. Aver, J. Gauss and J. F. Stanton, *J. Chem. Phys*., 2003, **118**, 10407–10417; (*b*) J. Gauss and J. F. Stanton, *Adv. Chem. Phys*., 2002, **123**, 355–373; (*c*) J. Gauss and H.-J. Werner, *Phys. Chem. Chem. Phys*., 2000, **4**, 2083–2090.
30 M. Milanesio, P. Ugliengo and D. Viterbo, *J. Med. Chem*., 1999, **42**, 291–299.
31 J. Dubois, D. Guenard, F. Guerette-Voegelein, N. Guedira, P. Potier, B. Gillet and J.-C. Beloeil, *Tetrahedron*, 1993, **49**, 6533–6544.
32 A. Lakdawala, M. Wang, N. Nevins, D. C. Liotta, D. Rusinska-Roszak, M. Lozynski and J. P. Snyder, *BMC Chem. Biol*., 2001, **1**, 2.
33 Q. Gao and S. H. Chen, *Tetrahedron*, 1996, **37**, 3425–3428.
34 J. K. Harper, J. Facelli, D. Barich, G. McGeorge, A. Mulgrew and D. M. Grant, *J. Am. Chem. Soc*., 2002, **124**, 10589–10595.
35 E. Pretsch, T. Clerc, J. Seibl and W. Simon, in *Tables of Spectral Data for Structural Determination of Organic Compounds*, Springer-Verlag, New York, 1989, 10–265.
36 J. K. Harper and D. M. Grant, *J. Am. Chem. Soc*., 2000, **122**, 3708–3714.
37 W. T. Dixon, *J. Chem. Phys*., 1982, **77**, 1800–1809.
38 A. E. Bennett, C. M. Reinstra, M. Auger, K. V. Lakshmi and R. G. Griffin, *J. Chem. Phys*., 1995, **103**, 51.
39 (*a*) D. W. Alderman, G. McGeorge, J. Z. Hu, R. J. Pugmire and D. M. Grant, *Mol. Phys*., 1998, **95**, 1113–1126; (*b*) N. K. Sethi, D. W. Alderman and D. M. Grant, *Mol. Phys*., 1990, **71**, 217.
40 B.-J. Van Rossum, H. Förster and H. J. M. de Groot, *J. Magn. Reson*., 1997, **124**, 516–519.
41 (*a*) M. Lee and W. I. Goldburg, *Phys. Rev. Lett*., 1963, **11**, 255–260; (*b*) M. Lee and W. I. Goldburg, *Phys. Rev. A*, 1965, **140**, 1261.
42 M. J. S. Dewar, E. G. Zoebisch, E. F. Healy and J. J. P. Stewart, *J. Am. Chem. Soc*., 1985, **107**, 3902–3909.
43 (*a*) A. D. Becke, *J. Chem. Phys*., 1993, **98**, 5648–5652; (*b*) J. P. Perdew and Y. Wang, *Phys. Rev. B*, 1992, **45**, 13224–13227.
44 M. J. Frisch, G. W. Trucks, H. B. Schlegel, G. E. Scuseria, M. A. Robb, J. R. Cheeseman, J. A. Montgomery, Jr., T. Vreven, K. N. Kudin, J. C. Burant, J. M. Millam, S. S. Iyengar, J. Tomasi, V. Barone, B. Mennucci, M. Cossi, G. Scalmani, N. Rega, G. A. Petersson, H. Nakatsuji, M. Hada, M. Ehara, K. Toyota, R. Fukuda, J. Hasegawa, M. Ishida, T. Nakajima, Y. Honda, O. Kitao, H. Nakai, M. Klene, X. Li, J. E. Knox, H. P. Hratchian, J. B. Cross, V. Bakken, C. Adamo, J. Jaramillo, R. Gomperts, R. E. Stratmann, O. Yazyev, A. J. Austin, R. Cammi, C. Pomelli, J. Ochterski, P. Y. Ayala, K. Morokuma, G. A. Voth, P. Salvador, J. J. Dannenberg, V. G. Zakrzewski, S. Dapprich, A. D. Daniels, M. C. Strain, O. Farkas, D. K. Malick, A. D. Rabuck, K. Raghavachari, J. B. Foresman, J. V. Ortiz, Q. Cui, A. G. Baboul, S. Clifford, J. Cioslowski, B. B. Stefanov, G. Liu, A. Liashenko, P. Piskorz, I. Komaromi, R. L. Martin, D. J. Fox, T. Keith, M. A. Al-Laham, C. Y. Peng, A. Nanayakkara, M. Challacombe, P. M. W. Gill, B. G. Johnson, W. Chen, M. W. Wong, C. Gonzalez and J. A. Pople, *GAUSSIAN 03 (Revision C.02)*, Gaussian, Inc., Wallingford, CT, 2004.
45 C. Jameson, in *Multinuclear NMR*, ed. J. Mason, Springer, New York, 1987, p. 56.
46 D. W. Alderman, M. H. Sherwood and D. M. Grant, *J. Magn. Reson., Ser. A*, 1993, **101**, 188–197.
47 J. K. Harper, G. McGeorge and D. M. Grant, *J. Magn. Chem*., 1998, **36**, S1354.
48 (*a*) R. A. Olsen, J. Struppe, D. W. Elliott, R. J. Thomas and L. Mueller, *J. Am. Chem. Soc*., 2003, **125**, 11784–11785; (*b*) M. T. Zell, B. E. Padden, D. J. W. Grant, S. A. Schroeder, K. L. Wachholder, I. Prakash and E. J. Munson, *Tetrahedron*, 2000, **56**, 6603–6616; (*c*) M. T. Zell, B. E. Padden, D. J. W. Grant, M. -C. Chapeau, I. Prakash and E. J. Munson, *J. Am. Chem. Soc*., 1999, **121**, 1372–1378; (*d*) G. De Paepe, A. Lesage, S. Steuernnagel and L. Emsley, *ChemPhysChem*, 2004, **5**, 869; (*e*) R. K. Harris, S. A. Joyce, C. J. Pickard, S. Cadars and L. Emsley, *Phys. Chem. Chem. Phys*., 2006, **8**, 137–143; (*f*) M. Strohmeier, J. K. Harper and D. M. Grant, presented at the 45th Experimental NMR Conference (Poster 398), 2004.
49 (*a*) B. Elena, A. Lesage, S. Steuernagel, A. Böckmann and L. Emsley, *J. Am. Chem. Soc*., 2005, **127**, 17296–17302; (*b*) B.-J. van Rossum, C. P. de Groot, V. Ladizhansky, S. Vega and H. J. M. de Groot, *J. Am. Chem. Soc*., 2000, **122**, 3465–3472; (*c*) E. Vinogradov, P. K. Madhu and S. Vega, *Chem. Phys. Lett*., 2002, **354**, 193–202; (*d*) B.-J. van Rossum, H. Förster and H. J. M. de Groot, *J. Magn. Reson., Ser. A*, 1997, **124**, 516–519; (*e*) S. Hafner and H. W. J. Spiess, *J. Magn. Reson., Ser. A*, 1996, **121**, 160–166; (*f*) P. K. Madhu, X. Zhao and M. H. Levitt, *Chem. Phys. Lett*., 2001, **346**, 142–148; (*g*) A. Lesage, S. Steuernagel and L. Emsley, *J. Am. Chem. Soc*., 1998, **120**, 7095–7100; (*h*) A. Lesage, D. Sakellariou, S. Steuernagel and L. Emsley, *J. Am. Chem. Soc*., 1998, **120**, 13194–13201.
50 W. C. Hamilton, in *Statistics in Physical Science*, The Ronald Press Company, New York, 1964, pp. 85–92.
51 J. K. Harper, N. K. Dalley, A. E. Mulgrew, F. G. West and D. M. Grant, *Acta Crystallogr., Sect. C*, 2001, **57**, 64–65.
52 J. C. Facelli, R. J. Pugmire and D. M. Grant, *J. Am. Chem. Soc*., 1996, **118**, 5488–5489.
53 E. A. Christopher, R. K. Harris and R. A. Fletton, *Solid State Nucl. Magn. Reson*., 1992, **1**, 93–101.
54 E. Graf, A. Kirfel, G.-J. Wolff and E. Breitmaier, *Liebigs Ann. Chem*., 1982, 376.
55 M. I. de Heer, P. Mulder, H. -G. Korth, K. U. Ingold and J. Lusztyk, *J. Am. Chem. Soc*., 2000, **122**, 2355–2360.
56 F. Gueritte-Voegelein, D. Guenard, L. Mangatal, P. Potier, J. Guilhem and M. Cesario, *Acta Crystallogr., Sect. C*, 1990, **46**, 781–784.
57 Q. Gao and W. L. Parker, *Tetrahedron*, 1996, **52**, 2291–2300.
58 T. Mukaiyama, I. Shiina, H. Iwadare, M. Saitoh, T. Nishimura, N. Ohkawa, H. Sakoh, K. Nishimura, Y. Tani, M. Hasegawa, K. Yamada and K. Saitoh, *Chem.–Eur. J*., 1999, **5**, 121.